Microzonation of Potenza (Southern Italy) in terms of spectral intensity ratio using joint analysis of earthquakes and ambient noise

Article *in* Bulletin of Earthquake Engineering · April 2012

DOI: 10.1007/s10518-011-9256-4

CITATIONS
28

READS
210

7 authors, including:

Leonardo Chiauzzi
Università degli Studi della Basilicata
37 PUBLICATIONS **636** CITATIONS
SEE PROFILE

Rossella Pagliuca
Università degli Studi della Basilicata
3 PUBLICATIONS **28** CITATIONS
SEE PROFILE

Marco Mucciarelli
National Institute of Oceanography and Applied Geophysics - OGS
276 PUBLICATIONS **5,474** CITATIONS
SEE PROFILE

Bull Earthquake Eng
DOI 10.1007/s10518-011-9256-4

ORIGINAL RESEARCH PAPER

Microzonation of Potenza (Southern Italy) in terms of spectral intensity ratio using joint analysis of earthquakes and ambient noise

Angelo Strollo · Stefano Parolai · Dino Bindi · Leonardo Chiauzzi · Rossella Pagliuca · Marco Mucciarelli · Jochen Zschau

Received: 30 September 2010 / Accepted: 26 February 2011

Abstract A temporary seismic network composed of 11 stations was installed in the city of Potenza (Southern Italy) to record local and regional seismicity within the context of a national project funded by the Italian Department of Civil Protection (DPC). Some stations were moved after a certain time in order to increase the number of measurement points, leading to a total of 14 sites within the city by the end of the experiment. Recordings from 26 local earthquakes (M_l 2.2−3.8) were analyzed to compute the site responses at the 14 sites by applying both reference and non-reference site techniques. Furthermore, the Spectral Intensity (SI) for each local earthquake, as well as their ratios with respect to the values obtained at a reference site, were also calculated. In addition, a field survey of 233 single station noise measurements within the city was carried out to increase the information available at localities different from the 14 monitoring sites. By using the results of the correlation analysis between the horizontal-to-vertical spectral ratios computed from noise recordings (NHV) at the 14 selected sites and those derived by the single station noise measurements within the town as a proxy, the spectral intensity correction factors for site amplification obtained from earthquake analysis were extended to the entire city area. This procedure allowed us to provide a microzonation map of the urban area that can be directly used when calculating risk scenarios for civil defence purposes. The amplification factors estimated following this approach show values increasing along the main valley toward east where the detrital and alluvial complexes reach their maximum thickness.

A. Strollo (✉) · S. Parolai · D. Bindi · J. Zschau
Helmholtz Centre Potsdam, GFZ German Research Centre for Geosciences, Telegrafenberg, 14473 Potsdam, Germany
e-mail: strollo@gfz-potsdam.de

A. Strollo
University of Potsdam, Karl-Liebknecht-Strasse 24, Haus 27, 14476 Potsdam, Germany

D. Bindi
Istituto Nazionale di Geofisica e Vulcanologia, Via Bassini 15, 20133 Milano, Italy

L. Chiauzzi · R. Pagliuca · M. Mucciarelli
DiSGG University of Basilicata, Viale dell'Ateneo Lucano, 85100 Potenza, Italy

Published online: 23 March 2011

Keywords Site effects · Seismic noise · Earthquakes · Spectral intensity · Correlation

1 Introduction

The city of Potenza is located in the Southern Apennines (Italy) and has currently 70.000 inhabitants (ISTAT demographic data, n.d.). Being the regional capital, during daytime it attracts from neighbouring villages a large number of commuters and students, reaching an estimated daytime occupancy exceeding 100.000 people. Over the last 30 years, 3 damaging earthquakes have affected this area. The M_s 6.9 Irpinia earthquake (1980) reached intensities of VII–VIII MCS inside the urban area of Potenza while the 1990 and 1991 earthquakes (respectively M_w 5.7 and M_w 5.2) yielded a maximum observed intensity of VI MCS (INGV Macroseismic Database, n.d). Furthermore, the city is located about 20 km from the "Pergola-Melandro" fault (Moro et al. 2007) which is situated between the maximum intensity areas of two of the most destructive earthquakes reported in the Italian seismic catalogue: the M $\sim$ 7.0 Val d'Agri earthquakes (1857) and the previously mentioned Irpinia earthquake. This fault is not associated with known historical events and for this reason is currently the subject of investigations as to whether it constitutes a potential seismic gap, where the probability of future ruptures may be higher than in the surrounding regions, also considering the static stress increase caused by the two above mentioned earthquakes (Lucente et al. 2005). Therefore, since the area encompassing Potenza and its surroundings are exposed to moderate to large earthquakes (in the magnitude range from 5 to 7), in the recently issued Italian seismic normative (INGV Italian Hazard map, n.d.), it has been included among the areas with the highest hazard level (i.e., classified as zone 1 according to the Italian seismic normative).

The city of Potenza was selected as a test site within the framework of the S3 Italian Civil Defence Department—National Institute of Geophysics and Volcanology 2004–2006 project (INGV DPC-S3, n.d.). The aim of this project was to calculate damage scenarios in areas of strategic and/or priority interest in Italy, starting from the maximum credible earthquake generated from surrounding seismogenic faults, and taking into account both site effects and building vulnerability. After the last damaging earthquake (1990), an extensive inventory in term of the vulnerability of buildings was collected within the framework of ENSeRVES project (European Network on Seismic Risk, Vulnerability and Earthquake Scenarios, Dolce et al. 2003). Several thousands of data sheets which include all necessary information were compiled through building by building field inspections, providing an additional data set for improved risk analysis.

In this work we first describe the geological setting of the investigated area and the data set acquired during the field surveys. Afterwards, by applying both reference and non-reference site techniques, we estimate the site response at sites where the earthquakes were recorded (henceforth referred to as the calibration sites) in order to assess the reliability of the NHV results. Spectral Intensity and the relative ratio with respect to the reference site have been also calculated and compared with amplification functions obtained from RSM methods for each calibration site. Using as a proxy the results of the correlation analysis performed between the NHV calculated for 233 single station noise measurements spread in the investigated area and those obtained for the 14 calibration sites, the SIR factors are exported to all measurement points. Finally, a microzonation map in terms of SIR is provided for Potenza.

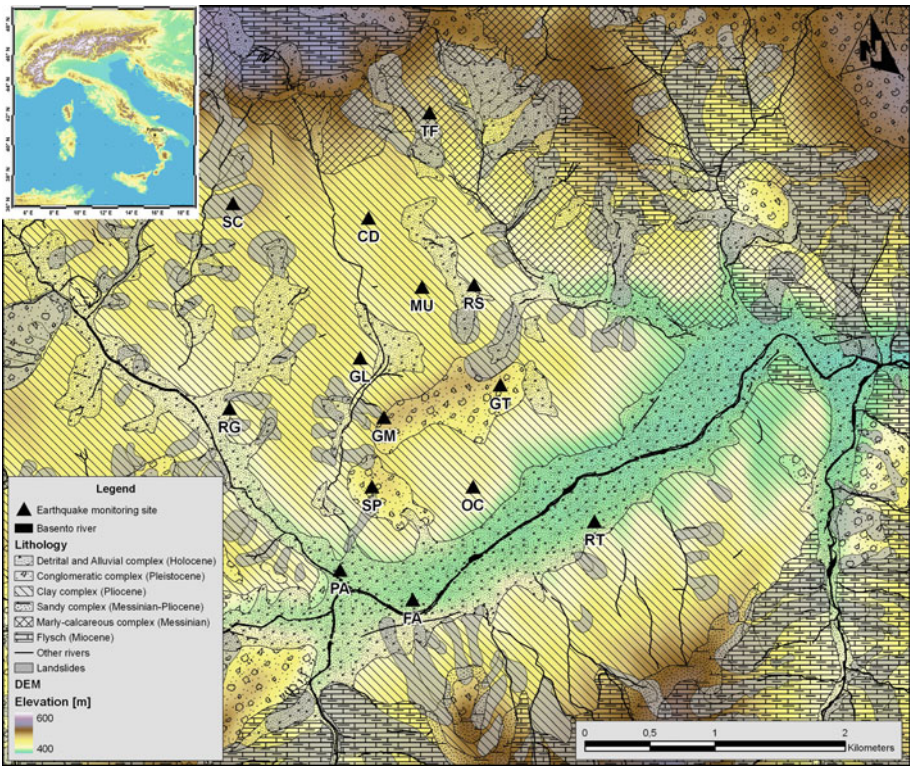

Fig. 1 Simplified lithological map. *The black triangles* indicate the location of the selected earthquake monitoring sites

2 Methodology

The effect that the local complex geomorphological features, such as the narrow valleys (covered by different kinds of soft sediments) surrounded by steep hills upon which the city lies (Figs. 1 and 2), have on ground motion amplification and duration must be taken into account for a reliable hazard assessment. These effects can be empirically estimated in terms of Fourier and spectral intensity amplification factors using both reference and non-reference site methods (Bard 1995). The reference site method (RSM), proposed by Borcherdt (1970), is based on the assumption that the spectral ratio of two recordings at nearby sites is directly related to the relative local site response since the path and source contributions are removed by the spectral division. This method can be generalized by jointly analyzing a set of earthquakes recorded by a local network (e.g., Andrews 1986; Castro et al. 1990; Bindi et al. 2006; Oth et al. 2008). The simultaneous spectral inversion of different earthquakes recorded by different stations, generally referred to as the generalized inversion technique (GIT), allows the separation of the contributions from the site from those of attenuation and the source. In many applications, it has been shown that if a suitable reference site is selected, the results provided by RSM and GIT are consistent (e.g., Steidl et al. 1996; Parolai et al. 2000; Bindi et al. 2009).

Since a reference site is not always available, techniques based on single station recordings, such as the horizontal-to-vertical spectral ratio (H/V) method, were introduced to estimate

site effects. This non-reference site technique was introduced first by Nogoshi and Igarashi (1971), but Nakamura (1989) made it popular. Originally, the method was proposed for interpreting ambient seismic noise measurements (NHV). Only later Lermo and Chavez-Garcia (1993), applied this technique to the S wave part of earthquake recordings (EHV), showing its capability to estimate the seismic resonance frequency of a site. Over the last few years, several studies have compared site responses obtained using reference and non-reference site techniques (e.g., Field and Jacob 1995; Parolai et al. 2004; Molnar and Cassidy 2006; Haghshenas et al. 2008). Most of them agree that RSM and EHV generally provide consistent estimates of the fundamental resonance frequency. However, the level of amplification, especially at frequencies higher than the fundamental one, might disagree. Also, the NHV method generally provides reliable estimates of fundamental frequency but not of the amplification of ground motion (Parolai et al. 2004).

Recently the engineering community has focused its attention on the spectral intensity (SI) (Housner 1952) as a tool to describe the severity of ground shaking. It has been shown that it is a stable estimator accounting for both the amplitude and frequency content of ground shaking (e.g. Ueong 2009; Masi et al. 2010). Recently Chiauzzi et al. (2011), following the approach of Housner (1952) developed a relationship between spectral intensity (SI) computed on data selected from the Italian accelerometric archive (Itaca, n.d.) and macroseismic intensities (EMS). This allows that the SI values can be easily used for calculating hazard and risk scenarios. Furthermore, when a reference site is available, the Spectral Intensity Ratio (SIR) with respect to a reference site can also be used as a description of the local site amplification (Pergalani et al. 1999; Marcellini and Pagani 2004; Pergalani et al. 2008). Importantly Marcellini and Pagani (2004) showed that the SIR range of variability is comparable with the range of soil correction coefficients prescribed by several seismic codes. In particular, with respect to the standard engineers practice in Italy, the design soil coefficient "S" that considers both soil conditions and topography (NTC08 n.d.) is directly comparable with SIR.

3 Geological setting

Potenza is located in Southern Italy, along the Apennines chain. It shows the typical features of villages and cities that have developed along this chain, with the old historical part located on the top of a hill and is surrounded by the more recent urban areas where the industries are generally located. In terms of seismic risk, the areas where the new settlements are developing are characterized by the largest exposure indexes, both in terms of population density and the presence of critical facilities. Figure 1 shows a simplified lithological map of Potenza, which has an extent of about 16 km^2 and elevation variations of about 200 m within the town.

Six different lithological units outcrop in the urban area. The basement of the most recent units dates back to upper Miocene, the period when the Apennine chain started forming. The flysch and the marly-calcareous complex are part of this basement and mainly belonging to the Lagonegresi unit (Di Nocera et al. 1988). These units surround the urban area and are essentially made up of layered calcarenites and varicoloured clays. The Plio-Pleistocene units lying on the basement and outcropping in the central part of the map belong to the Altavilla and Ariano units, and are mostly made up of sands, grey-blue silty clays and conglomerates. The uppermost sediments (Holocene), referred to as detrital and alluvial complexes in the simplified geological map above consist of mainly silty and clayey alluvial debris and deposits. In Fig. 1, the location of landslides is also indicated, showing that, as discussed in Caniani et al. (2008), about 30% of the urban territory is prone to slope instability. It is worth noting

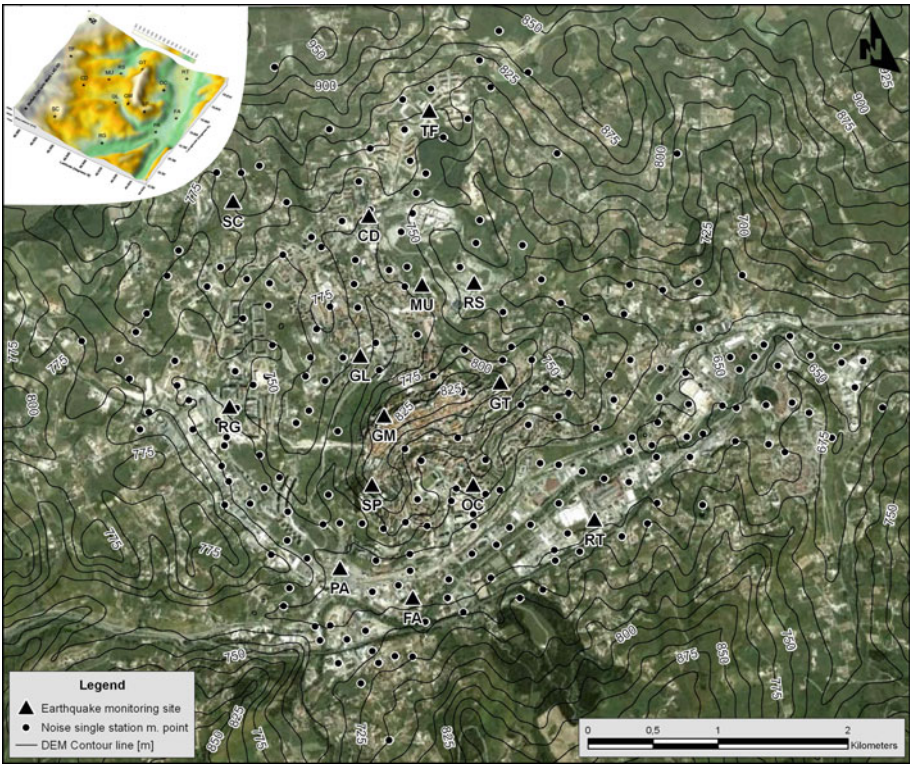

Fig. 2 Seismic stations (*triangles*) and single station noise measurement points (*circles*) locations within the city of Potenza. The inset shows the 3D digital elevation model

that almost all the landslides detected are located inside the clay complex (Ariano Unit) and within the flysch and the marly-calcareous complex (Lagonegresi unit) at the detachment interface between layered calcarenites and varicoloured clays.

4 Data set

A seismic network composed of 11 stations was installed in Potenza and operated from October 2004 to May 2005. The number of investigated sites was increased to 14 (shown as black triangles in Figs. 1 and 2) by moving some stations to different sites during this period.

In particular, one station was moved, after 1 month of acquisition, from the SC to GL sites (Fig. 1) and moved again from GL to OC 2 months before the end of the experiment. A second station was moved from site PA to RT, after an acquisition period of 4 months. The monitoring sites were selected with the aim of sampling different characteristic units from both geological and geomorphological points of view. Particular attention was dedicated to areas damaged by past earthquakes. The stations, installed always in the ground floor of buildings, were equipped with a 24 bit digital acquisition system, a 1 Hz natural frequency calibrated geophone, and GPS antenna for synchronous time and position recording.

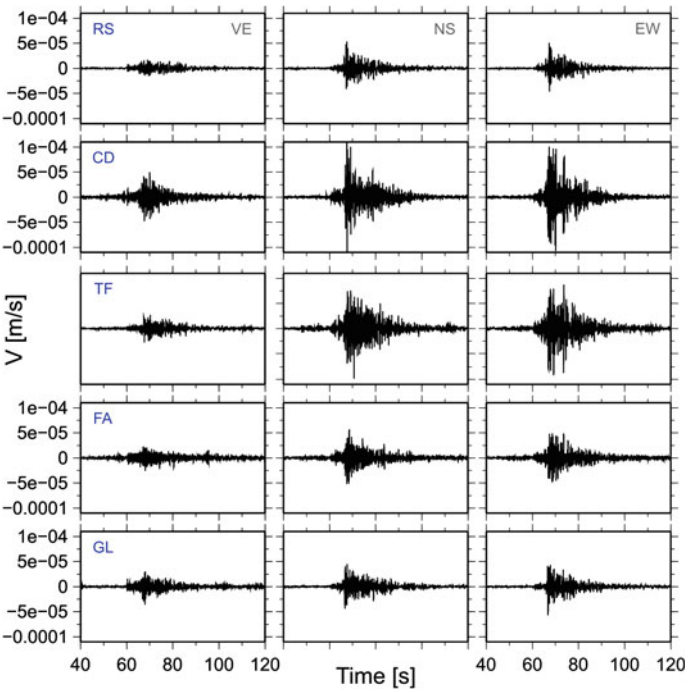

Fig. 3 Example of recordings of a M_l 2.8 earthquake that occurred at ∼ 50 km from the network (Fig. 4). In the *left*, *middle* and *right* panels are represented the vertical, north-south and east-west components, respectively. The station code (Fig. 1) is provided within each frame in the left column

The sampling rate was fixed to 100 sps and recording was continuous mode. During the monitoring period, about 250 earthquakes, including local, regional and teleseismic events, were recorded. The recordings from 26 local earthquakes with signal to noise ratios greater than 3 over the frequency range 1–10 Hz were selected for evaluating site effects in Potenza. The selected earthquakes span the local magnitude range from 2.2 to 3.8 and the distance range from 5 to 71 km. For each earthquake recording, a pre-event noise window of 30 min was also stored. In Fig. 3, the recordings from the three components at 5 different stations of a $M_l = 2.8$ earthquake located ∼50 km from the network are showed. It is worth noting the relative amplification of the peak ground velocity at sites CD and TF with respect to RS.

In order to perform the following analysis, for the local subset of events, P- and S-phase arrivals were identified and used to re-locate the selected earthquakes using Hypoellipse (Lahr, n.d.). Since the aperture of the network was not enough large to provide satisfactory locations (Fig. 4), arrival times from 13 permanent stations deployed in the region that belong to the INGV-MedNET network (NGV-MEDnet, n.d.), were also used. The model used for the location is outlined in Table 1.

During the working period of the network, 233 single station noise measurements were carried out within the urban area of Potenza (Fig. 2), sampling different lithologic and topographic conditions. For each site, 30 min of ambient noise was recorded using a 24 bit digital acquisition system with an embedded 4.5 Hz three component geophone. The sampling rate was set to 100 sps.

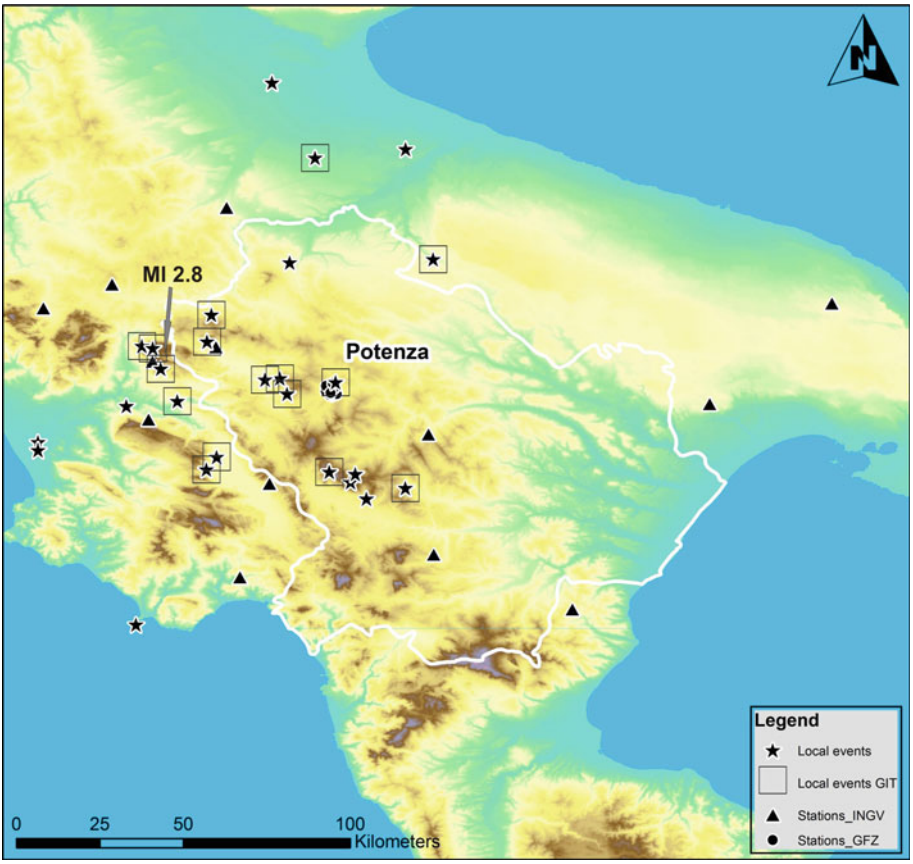

Fig. 4 The temporary seismic network in Potenza (*circles*); the local events used in this study are represented with *the star* while only those with the *black square* have been used for GIT. *Triangles* indicate the INGV-MedNET permanent stations used for re-locating the events. *The gray arrow* indicates the epicentre of the event showed in Fig. 3

Table 1 Seismic velocity model used for locating the local events showed in Fig. 4

Vp [km/s]	h [km]
3,0	1,0
3,5	2,0
4,5	5,0
5,2	10,0
6,0	30,0
8,1	Halfspace
Vp/Vs fixed to 1,73	

5 Earthquake horizontal to vertical spectral ratio (EHV)

The EHV method belongs to the class of so-called non-reference site methods (Bard 1995). It is based on the assumption that the vertical component of ground motion is not affected by amplification effects during the propagation through the soil layers and that it is similar

to the horizontal component at the bedrock. The spectral ratios were carried out considering windows selected with the criteria that they contain 90% of the energy content for both P and S phases. The largest duration among those obtained for three components has been considered to have the same length over the three components. For local events, the P-wave window ended 1 s before the S-wave arrival (if the 90% of energy is not reached yet) while the maximum duration for the S-wave windows was fixed to 90 s. Each window has been cosine tapered (5%) and Fourier transformed. Instrumental corrections have been applied and the spectral amplitudes smoothed using a Konno and Ohmachi (1998) window. The parameter b, which determines the degree of smoothing, was fixed to 40, ensuring the smoothing of numerical instabilities while preserving the major features of the spectra. Finally, the root-mean-square of the two horizontal components has been computed and, for each station, the geometrical mean of the horizontal-to-vertical spectral ratios for different recordings has been evaluated. Depending upon the period of operation and gaps in the functioning of the stations, the number of events considered for computing the Horizontal to Vertical Spectral ratios varies from 6 (station SC) to 26 (station RS, see Fig. 1). Figure 5 exemplifies the EHV for 6 stations that are representative of the results obtained for the calibration sites in Potenza. The results show that EHV obtained for RS and RG stations (Fig. 5, first row) are almost flat. These stations were installed over the silty-clay complex (Fig. 1), the most common lithology within the city, and where the S-wave velocity has been estimated to be higher. Moreover, since station RS was installed within the draining tunnel of the university, at about 6 m below ground level, good quality recordings are available for this station for almost all the considered events, due the less noisy environment with respect to the other stations. For all the above reasons, in the following analysis station RS is used as the reference station. The others stations shown in Fig. 5 (MU, TF, CD and RT) show significant peaks in their amplifications in the frequency range from 2 to 5 Hz, with a good agreement between the results obtained for P- and S-wave windows. MU and CD sites are located on the silty-clay complex while TF site lies within the marly-calcareous complex on a large landslide. In this case, the peaks observed in the spectral ratio can be related to the landslide's detachment surface. Finally, RT site is located along the valley filled by the detrital and alluvial complexes. These sediments have a thickness ranging from 0 to some tens of meters, reaching a depth of about 25 m at the RT site.

The results for the remaining stations, as well as the signal to noise ratio, are shown in the Appendix.

6 Standard spectral ratio (SSR)

The SSR technique is also a reference site method (Bard 1995). In fact, once a reference site has been chosen, the spectral ratios between all the other stations and the reference are calculated for each component of ground motion. In this work, we compute the SSR with respect to station RS and analyze the same S-wave windows used for computing the EHV. In Fig. 6, the SSR for the horizontal components of 5 representative stations are shown (the same sites as in Fig. 5, but without RS). The remaining sites are presented in the Appendix. A general good agreement between the EHV (Fig. 5) and SSR results is observed, both in terms of the locations of peaks and the amplification levels. In particular, the SSR results confirm that RG has an almost flat amplification function, while stations TF, CD and RT show peaks in their amplification in the frequency range between 2 and 5 Hz.

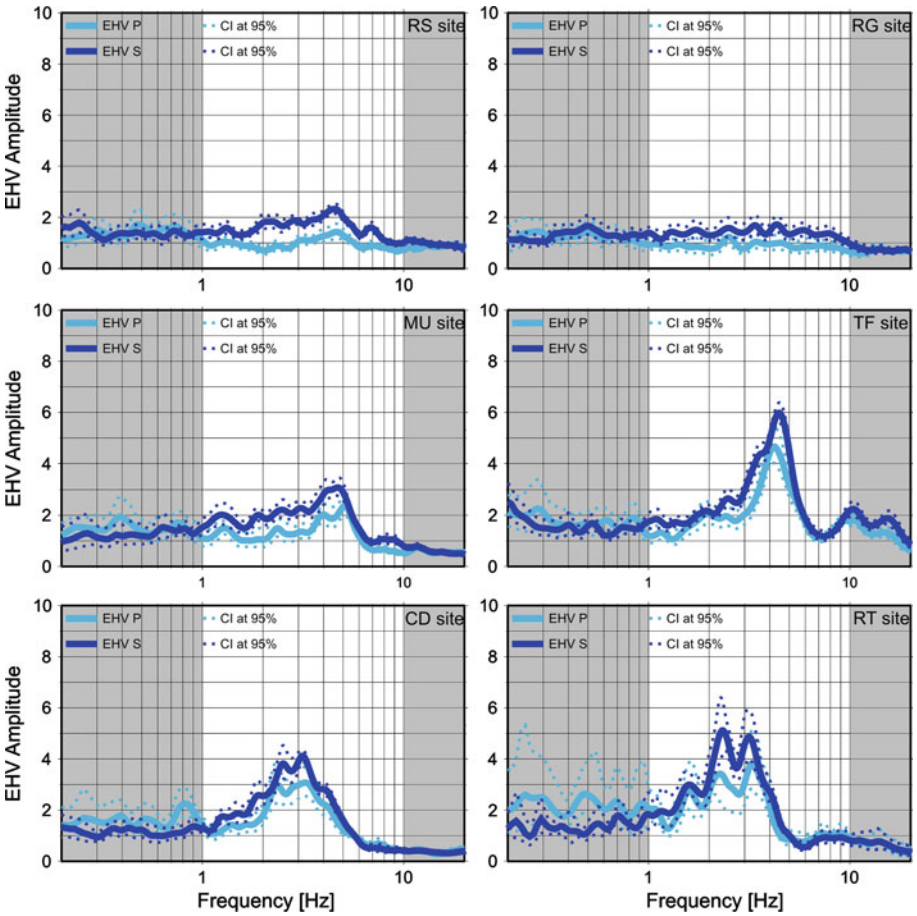

Fig. 5 EHV for 6 different sites. *The blue* and *the light blue lines* represent the EHV calculated using the S phase and P phase windows, respectively. The two *thin dotted lines* represent the 95% confidence interval. *The gray shadowed* areas indicate the frequency band where the signal to noise ratio is smaller than 3

The shift of the frequency corresponding to the amplification peak observed in the SSR for station MU with respect to the EHV is related to the amplification affecting the vertical component, as shown in Fig. 6.

7 Generalized inversion technique (GIT)

In the GIT method, the site response of all stations are simultaneously separated from the source spectra and attenuation function by performing a matrix inversion (e.g., Castro et al. 1990; Parolai et al. 2004; Oth et al. 2008) The natural logarithm of the spectral amplitudes $U_{ij}\,(f, r)$ for an event i observed at a recording site j, can be described as:

$$\ln U_{ij}(f, r) = \ln S_i(f) + \ln Z_j(f) + \ln A_{ij}(f, r) \tag{1}$$

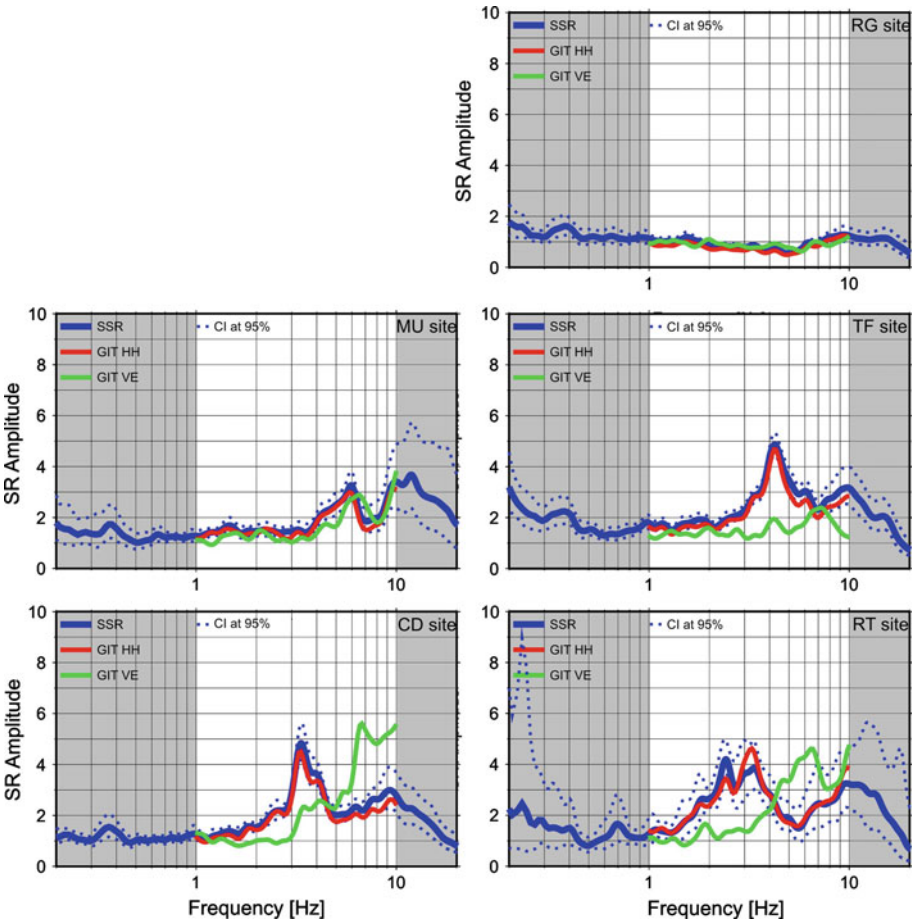

Fig. 6 SSR and GIT results for 5 sites (the name of the site is indicated in the upper-right part of each panel). *The blue lines* represent the SSR with its 95% confidence interval while *the red and the green lines* represent the GIT for the horizontal component, and for the vertical component, respectively. *The gray shadow* indicates the frequency band with a signal to noise ratio smaller than 3

where $S_i\,(f)$ is the source spectrum, $Z_j\,(f)$ is the site response, $A_{ij}\,(f, r)$ is a function accounting for attenuation along the path, f is the frequency and r is the distance. For all events and all stations, Eq. (1) describes a linear system of the form $Ax = b$, which can be solved by using suitable inversion algorithms. In order to avoid *a priori* parameterization of the attenuation term $A_{ij}(f, r)$, the inversion is generally performed in two steps (Castro et al. 1990). In the first step, the inversion is carried out to separate the source and attenuation effects. The trade-off between attenuation and source is resolved by requiring that the attenuation assumes an *a priori* value at a given distance, irrespective of frequency. In the second step, the inversion is carried out for the source function and the site responses, using residuals obtained for correcting the observed data for the attenuation results. The undetermined degree of freedom of the second inversion is resolved by constraining the logarithm of the site amplification of the reference station to 0, irrespective of frequency.

Since the distribution of recordings versus distance does not allow a reliable seismic attenuation function to be derived over the analyzed distance range, in this study we carry out only the second step of the inversion after having corrected the observed spectral values, relevant to the 16 earthquakes for the attenuation effects (Luzi et al. 2005). We considered a regional model previously derived for the studied area (Castro et al. 2004) that follows the form:

$$A(f, r) = \frac{1}{R} e^{-\frac{\pi f R}{Q\beta}} \tag{2}$$

where R is the hypocentral distance, f the frequency, β the shear wave velocity (assumed to be 3.5 km/s), and $Q(f) = 32.1 f^{1.7}$ is the frequency dependent quality factor. Previous studies (e.g. Parolai et al. 2000) have shown that this choice does not affect the site response estimation.

The GIT inversion has been carried out over the frequency range 1–10 Hz where the signal-to-noise ratio is greatest. The site responses for the horizontal components obtained for stations RG, MU, TF, CD and RT are shown in Fig. 6. Since for the GIT the amplification function of RS site was constrained to 1 irrespective of frequency, the good agreement between SSR and GIT results shown in Fig. 6 confirm that RS is a suitable reference site, almost free from significant amplification effects. A very good agreement between SSR and GIT for vertical components has been observed as well although here only the GIT results for the vertical component have been showed. In particular the peaks at about 6 Hz on the vertical component in Fig. 6 explain the strong de-amplification in the EHV for RT and CD sites showed in Fig. 5. The GIT transfer functions obtained for all the stations are shown in the Appendix.

8 Seismic noise horizontal to vertical spectral ratio (NHV)

The horizontal-to-vertical spectral ratio method was also applied to ambient noise recordings (NHV). Differently from the EHV, SSR and GIT methods, the analysis of noise was carried out using the seismic noise recordings from both the calibration sites and from the other 233 sites selected within the urban area. For each of these sites, we analyzed 20 non-overlapping signal windows with a duration of 60 s. Each window was tapered at both ends with a 5% cosine taper and its Fast Fourier Transform (FFT) calculated. The FFT have been smoothed using a Konno-Ohmachi window (Konno and Ohmachi 1998) fixing the parameter b to 40. For each 60 s window, the NHV was computed and the logarithmic average of the NHV estimated. The good agreement between the NHV, EHV and SSR results shown in Fig. 7 for the sites RS, RG, MU, TF, CD and RT confirm that, through the analysis of ambient noise, it is possible to capture the main features of the amplification effects over the considered frequency band.

9 Spectral intensity ratio (SIR)

In order to calculate the SIR for each site with respect to the reference site, spectral intensity (SI) has been calculated for each local event. Although in the original definition of Housner (1952) the SI is calculated as the area under the pseudo-velocity spectrum (PVS) between the periods of 0.1 and 2.5 s, in this paper, following (Gavarini and Gruppo di lavoro 1999), a different integration interval (0.2–2 s, (0.5–5 Hz) according to Eq. 3) was used in order to

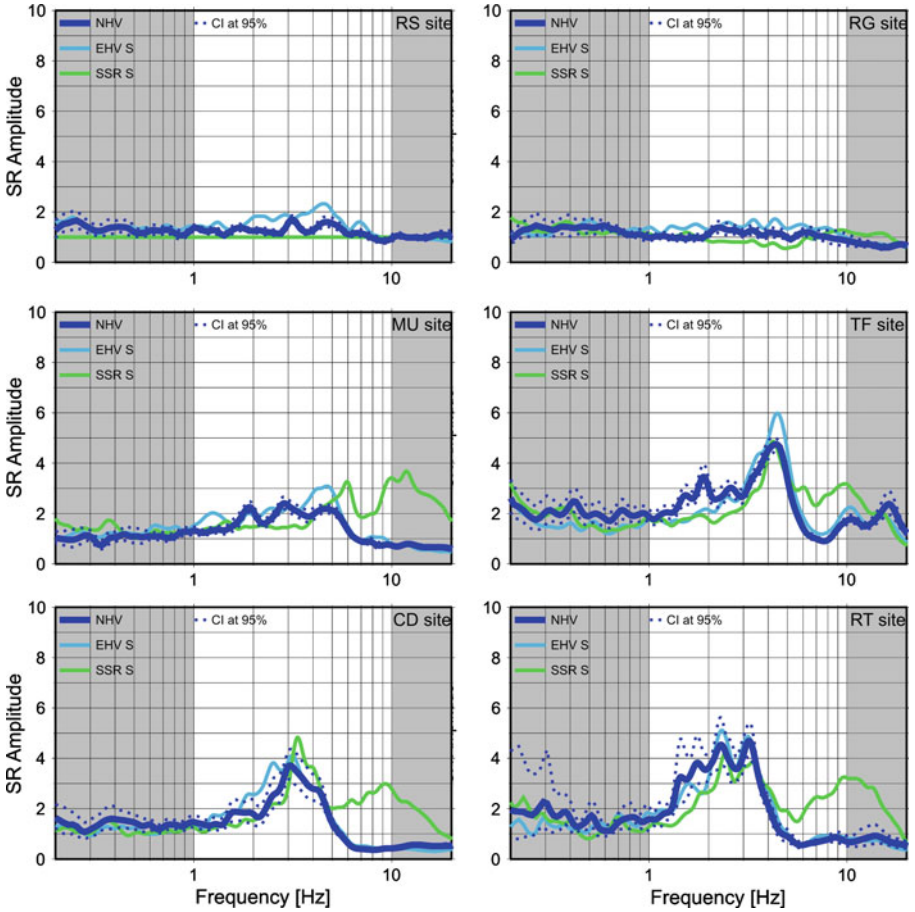

Fig. 7 NHV results (*thick blue line*) with their 95% confidence interval (*dotted blue line*). EHV and SSR results are showed in light blue and green, respectively. *The gray shadowed* areas indicate the frequency band with signal to noise ratios for EHV and SSR smaller than 3

take into account both the frequency band with sufficient signal to noise ratio for the recorded events and the period of vibration of modern building stock (Gallipoli et al 2010).

$$SI = \int_{0.2}^{2} PVS(T,\xi)dT \tag{3}$$

In fact, considering the characteristics of the Italian buildings, it was shown that SI calculated within this interval provides a better correlation with the building damage grade in terms of EMS Intensity scale (Gavarini and Gruppo di lavoro 1999 and Chiauzzi et al. 2011). Response spectra were calculated considering a 5% of the critical damping. For each earthquake, the maximum between the ratio of the two horizontal components with respect to the SI evaluated for the reference site has been retained as being representative of the site. Finally, for each calibration site (i.e., where earthquakes have been recorded), the SIR factor has been computed as the median of the distribution of values obtained considering different

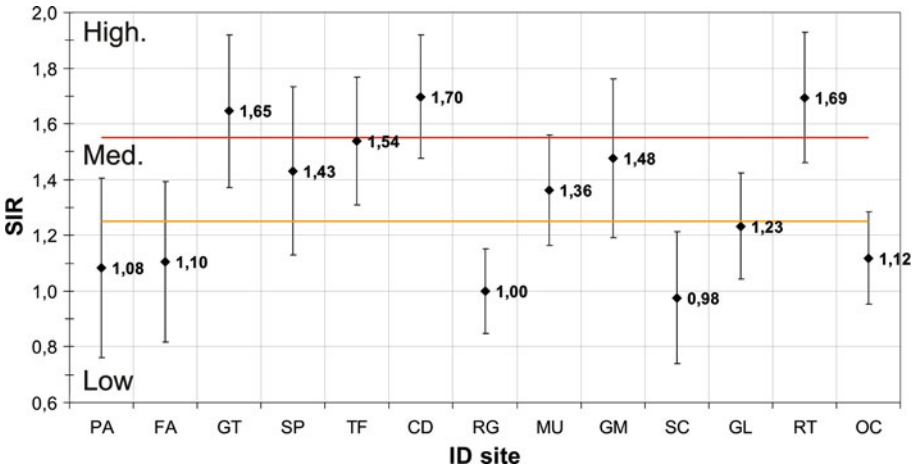

Fig. 8 Spectral intensity ratios (*SIR*) obtained for the 13 calibration sites with respect to station RS. The median ± one standard deviation is shown for each station. *The orange* and *the red lines* separate the SIR values into three classes with respect to the amplification level

earthquakes (Fig. 8). The largest SIR values are obtained for those stations affected by significant amplification effects over the frequency range 0.5–5 Hz (corresponding to the period interval used in Eq. 3), such as stations RT and CD (Fig. 7). The obtained SIR coefficients are in turn used to group the stations into three classes of amplification (low, medium, and high) using a cluster analysis (Tryon 1939), as shown in Fig. 8.

10 Correlation analysis and microzonation map

Recently, different attempts to correlate the NHV function with the site response have been carried out. Bragato et al. (2007), following the approach used by Rodriguez and Midorikawa (2002), used NHV functions to identify homogeneous areas in terms of site response by means of cluster analysis, following a Bayesian approach. Similarly Cara et al. (2010), used the correlation between NHV functions and local geology to explain the damage pattern of a past earthquake in Palermo (Italy). In both studies, the sites are clustered by considering similarity in the NHV function, but without associating any site response function calculated using earthquake data to each cluster.

In the previous sections, the reliability of the NHV functions and SIR values in representing a proxy for separating areas affected by different site effects occurring at the calibration sites in Potenza was assessed through direct comparisons with GIT and SSR results. In particular, independent of the shape, sites showing similar SSR results also share similar NHV curves. It follows that the NHV functions can also be used as a tool that allow the extrapolation of the SIR values computed at the calibration sites to all the other sites in Potenza where the ambient noise has been measured.

In this work, we applied a correlation approach to NHV following two main steps:

(1) The degree of similarity between the NHV functions estimated at noise measurement points with the calibration sites is quantified by considering the product between the Pearson cross-correlation coefficient (Eq. 4) (Davis 1986) and the degree of fit (Eq. 5):

$$r_{jk} = \frac{cv_{jk}}{\sigma_j \cdot \sigma_k} = \frac{\left(\frac{\sum_{i=1}^{n}(x_{ij}-\overline{x}_j)\cdot(x_{ik}-\overline{x}_k)}{(n_i-1)}\right)}{\left(\sqrt{\frac{\sum_{i=1}^{n}(x_{ij}-\overline{x}_j)}{(n_i-1)}}\right)\cdot\left(\sqrt{\frac{\sum_{i=1}^{n}(x_{ik}-\overline{x}_k)}{(n_i-1)}}\right)} \tag{4}$$

$$f_{jk} = \frac{1}{\sqrt{\frac{\sum_{i=1}^{n}(x_{ij}-x_{ik})^2}{n_i}}} \tag{5}$$

In these equations, $\boldsymbol{i}$ represents the number of frequencies selected over the range 1–10 Hz (740 samples), $\boldsymbol{j}$ is the number of noise measurement sites (233), $\boldsymbol{k}$ is the number of calibration sites (14) and the vector x represents the NHV functions. The selected frequency range accounts for both the limits of the instruments (i.e. 4.5 Hz geophone) used for measuring ambient noise (e.g., Strollo et al. 2008) and the range of variability of the fundamental frequency of resonance computed in the previous sections for Potenza. Moreover, the upper limit was fixed to 10 Hz in order to avoid strong and very local high frequency sources of noise that are quite common in urban and industrial environments.

A cross-correlation matrix CC is then evaluated as

$$\mathrm{CC} = r \cdot f \tag{6}$$

where the matrix CC has dimension [233 × 14].

In order to identify at which calibration site the noise measurement point is closer in terms of NHV similarity, a threshold of positive values of CC larger than 0.3 has been chosen (existence condition). Moreover, a difference in amplitude of at least 10% between the two largest values in the matrix CC for each noise measurement site was required in order to identify uniquely the corresponding calibration site (uniqueness condition).

(2) In the second step, the noise measurement points that did not satisfied the uniqueness condition were associated with one of the possible selected calibration sites by considering a hierarchical scheme based on considering the largest value of the CC coefficient, the lithological properties and the distance to the calibration sites with the higher CC values. In particular, among the calibration sites showing CC values within the 10% of the highest one, the noise measurement point is associated with the closest one that shares the same lithology. If the closest among these calibration sites are within 10% of the max CC value and share the same lithology at a distance larger than 1 km, the noise measuring point is excluded.

Figure 9 exemplifies the results for two different noise measurement points. In each panel, the NHV evaluated for the site (blue line) and those relevant to the calibration points with both the largest (light blue line) and smallest (gray line) cross-correlation coefficients are shown. The example shown in the left panel represents a case corresponding to one of the largest cross correlation obtained (CC=3.6) while the example in the right panel correspond to a cross-correlation value equal to the threshold select for the existence condition (CC=0.3). Figure 9 show that also in the case of the minimum adopted threshold value a fair agreement between the NHV curves is observed.

By applying the two-step cross correlation scheme, SIR values have been successfully associated with 213 sites in Potenza, allowing us to produce a map of 227 SIR values spread within the town (Fig. 10).

Finally, since for engineering applications such as land-use planning or risk scenario computations, the identification of homogeneous macro-areas within an urban territory with respect to the level of expected ground motion is required, the 227 SIR values were

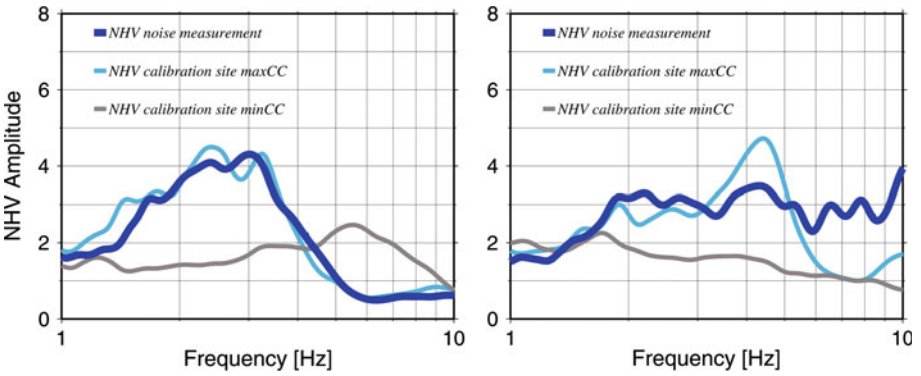

Fig. 9 Two examples of correlation (points n. 202 (*left*) and 125 (*right*) indicated in Fig. 10): NHV of the noise measurement point in blue and NHV for the associated calibration site in *light blue*. *The grey line* represents the NHV of the calibration site with the lowest correlation coefficient. *Left and right* panel have been selected respectively between the maximum and minimum values of correlation coefficients. The *NHV* of the calibration sites having the max CC values for the two measurements, 202 and 125 are respectively RT and TF, while the min CC values are respectively SC and SP

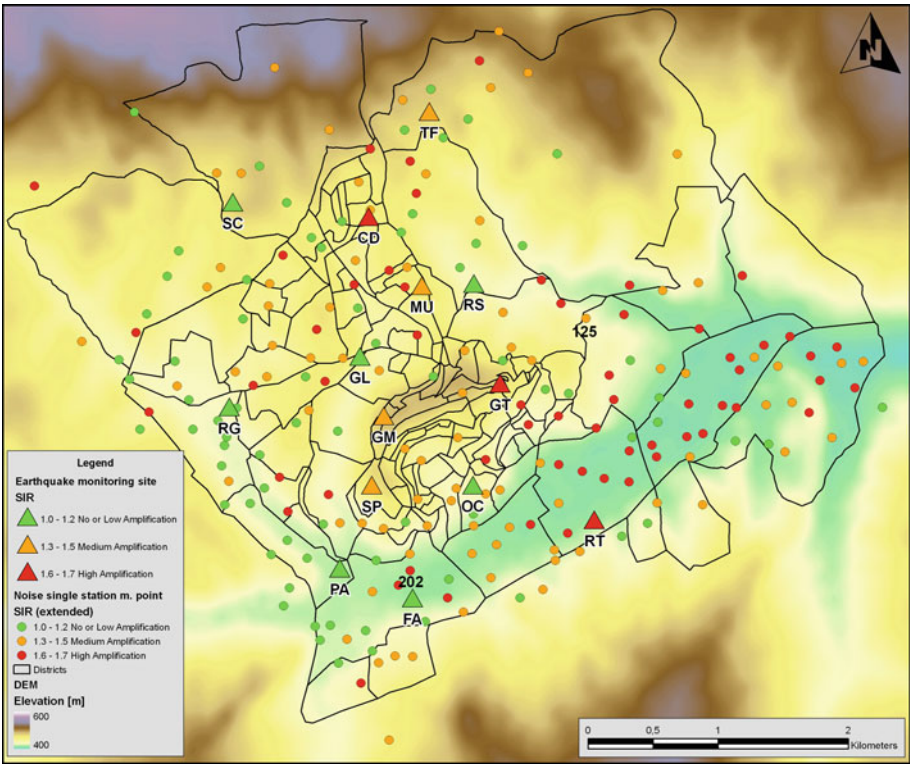

Fig. 10 Distribution of SIR values for both earthquake monitoring sites and those used for the noise measurements points

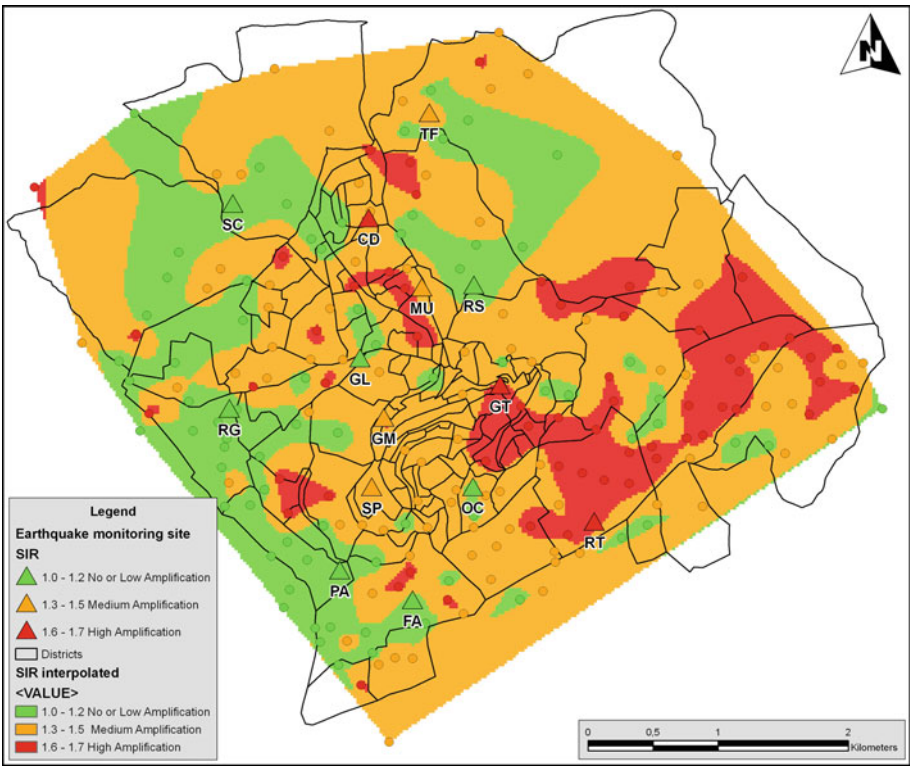

Fig. 11 Natural neighbours interpolation of the SIR values

interpolated (Fig. 11) and macro areas identified. The SIR values are represented in the map according with the three classes identified by means of the cluster analysis (Fig. 8).

11 Discussion and conclusions

Within the framework of the seismic microzonation of the town of Potenza (Southern Italy), we have introduced a procedure to extrapolate and link the acquired information, calibrated at a small number of high-quality recording sites, to a larger number of points within the town.

The approach followed in this work can be described in three steps as follows (Fig. 12). In the first step, the site transfer functions of 14 sites (calibration sites) in the town, where a temporary seismic network was installed, have been computed using the recorded earthquakes. We applied different techniques to the spectra of S-wave computed for both horizontal and vertical components. A good agreement was obtained between the results of the horizontal-to-vertical spectral ratio technique (EHV) and the site response evaluated by computing the spectral ratios with respect to a reference rock site (SSR and GIT methods). In Potenza, the fundamental frequency of resonance varies within the frequency range from 2 to 6 Hz, with amplifications of up to 6. Differences observed for a few sites (e.g. station MU) can be

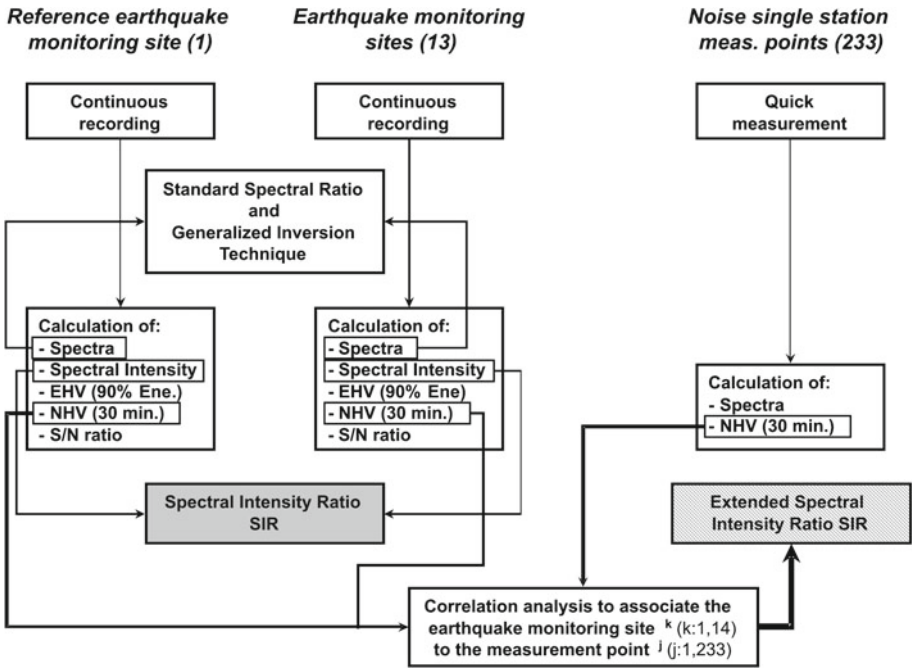

Fig. 12 Flow-chart of the procedure applied in this study to provide a microzonation of Potenza in terms of Spectral Intensity Ratios

ascribed to amplifications affecting the vertical component. Moreover, the good agreement between EHV calculated using P and S waves suggests that S-to-P phase conversion could contaminate the wave-field of the horizontal component within the selected P window as showed by Parolai and Richwalski (2004).

In the second step, a single parameter (i.e., spectral intensity ratio) that captures the amplification over the frequency range of interest and well correlates with macroseismic intensity has been introduced to describe the site effects at the calibration sites. The reliability of SIR as a measure of site amplification effects has been assessed by comparing the spatial variation of the SIR values with that of the site response. We observed that sites showing larger amplification (4–6) also have larger SIR values (1.6–1.7) and that the SIR values vary with the amplification functions.

Finally, in the third step, a procedure to extrapolate and link the SIR values to other sites in Potenza, where recordings of earthquakes were not available, was proposed. Since ambient noise has been recorded at 233 sites in Potenza, we first assessed the suitability of the horizontal-to-vertical spectral ratio of ambient noise (NHV) as tool to estimate the site amplification variability. This task has been accomplished by computing the NHV at the monitoring sites and comparing the results with those of SSR. The good agreement shown by the results obtained from the analysis of noise and earthquakes confirmed that the NHV method is a suitable tool (at least in Potenza) to capture the significant features of site responses and their spatial variability. Then, we used the NHV as a proxy to extrapolate amplification factors (SIR) estimated at the calibration sites to a large number of sites within the town where only noise recordings were available. We developed an approach based on cross-correlation applied to NHV to identify, for each considered site, the calibration site closest in term of site

response. Following this approach, we were able to generate a microzonation map (Fig. 10) for Potenza in terms of Spectral Intensity Ratio values.

This map shows increasing amplification factors along the main valley, starting from nearly no amplification surrounding the RG site at its apex and increasing towards the RT site where the valley is widening (Figs. 2 and 10). The amplification factors reach a maximum in eastern side of the investigated area where detrital and alluvial complexes reach their maximum thickness. Large amplification factors are also surrounding the GT site. Others isolated spots correlate well with existing landslides like the red area located on the eastern side with respect to RS site and red spots aligned between SC and GM sites. Medium amplification factors can be assigned to the remaining part of the urban area except for some green areas including RS, GL, OC and SC sites with low amplification. These variations in amplification are related to lateral changes within the clay complex that is composed of clays with different grades of consolidation. The SIR zonation (Fig. 11) shows a fair correlation with the main features of the lithological map (Fig. 1), indicating that the general of the variations in ground motion are related to lithological changes. The largest amplifications were also observed to correspond to the area covered by the new settlements, industries and strategic facilities (south-east part of the town). Site effects must be therefore taken into account when assessing the seismic risk for this strategically important area.

Finally, we proposed a method for seismic microzonation, based on combining two different layers of information. The first layer includes detailed but sparse information obtained from the analysis of earthquake data, such as site responses and SIR amplification factors. The second layer includes NHV functions of the elements included in the first layer as well as a large number of additional points to improve spatial resolution. Subsequently, the two layers are linked through similarities in the NHV functions.

Importantly we should remark that the SIR correction factor (accounting for site amplification effects) has been easily included in the hazard scenarios generated for assessing seismic risk in Potenza, improving the spatial resolution and ground motion estimation. In fact, in a first attempt at producing a complete scenario for damage assessment in Potenza using three scenario earthquakes (Chiauzzi et al. 2011), used relationship between Spectral Intensity (SI) and Macroseismic Intensity (EMS) for generating the seismic input. This was in turn locally modified using our site specific coefficients. The results show that, considering site effects, the estimation of unusable buildings in the event of the scenario earthquake increases by 50%. This confirms the potential of the proposed approach for improving seismic risk scenarios for large urban areas.

Acknowledgments Dr. K. Fleming kindly revised our English. Part of this research has been funded within the DPC-INGV-S3 project. Part of the figures presented in this manuscript has been generated using the GMT software package (Wessel and Smith 1991).

Appendix

Spectral ratios and signal to noise ratio for all the stations used in this paper

See Figs. 13, 14, 15, 16, 17, 18, 19, 20, 21, 22, 23, 24, 25 and 26

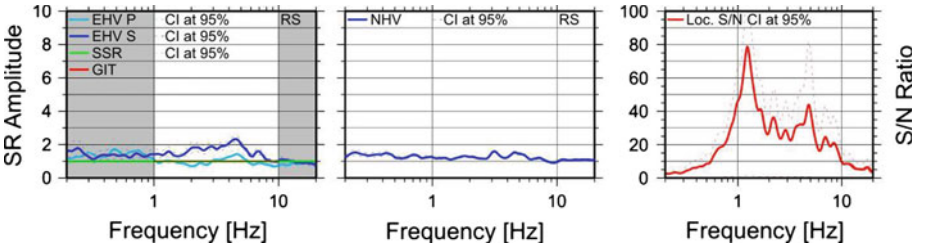

Fig. 13 Standard spectral ratio for RS site. *Left panel*, *EHV* calculated for both P and S phases respectively showed in *light blue and blue*; *SSR* and *GIT* are represented respectively in *green and red*. *The gray* shadow indicate the frequency band with signal to noise ratio smaller than 3. *NHV* is showed in the central panel. *Right panel*, average signal to noise ratio of the events used

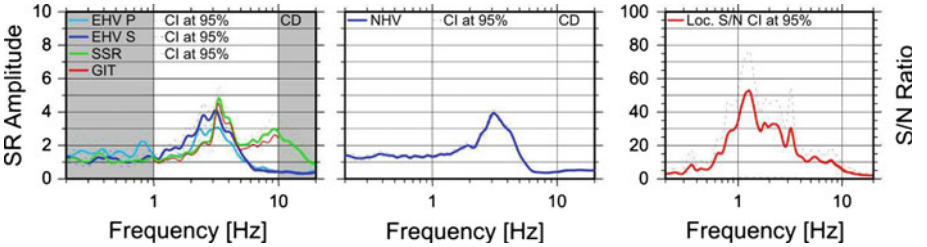

Fig. 14 Same as Fig. 13 but for site CD

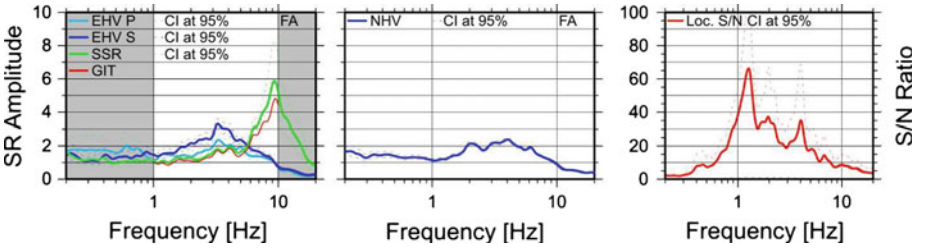

Fig. 15 Same as Fig. 13 but for site FA

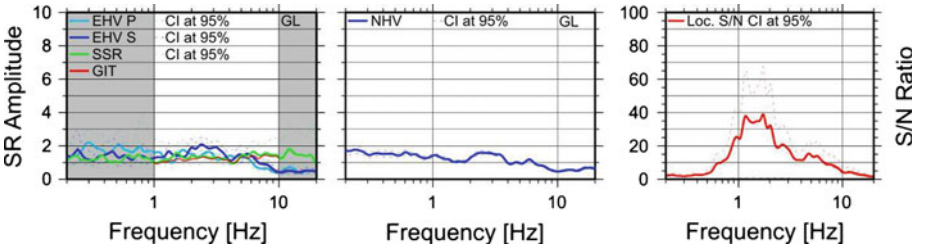

Fig. 16 Same as Fig. 13 but for site GL

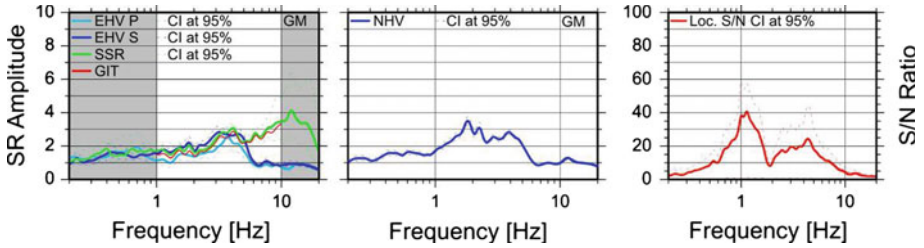

Fig. 17 Same as Fig. 13 but for site GM

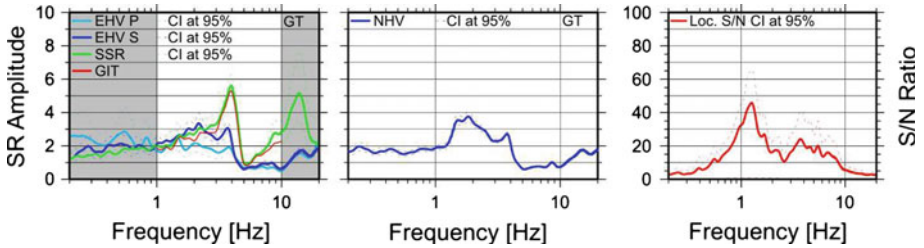

Fig. 18 Same as Fig. 13 but for site GT

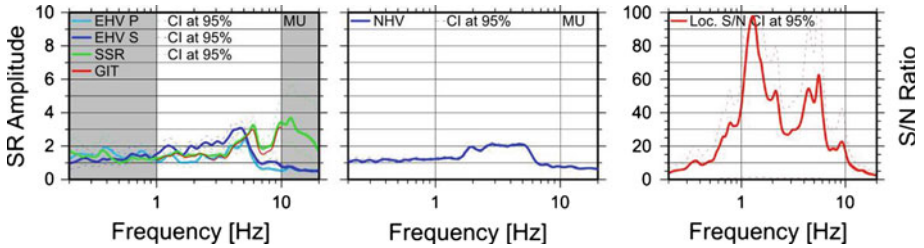

Fig. 19 Same as Fig. 13 but for site MU

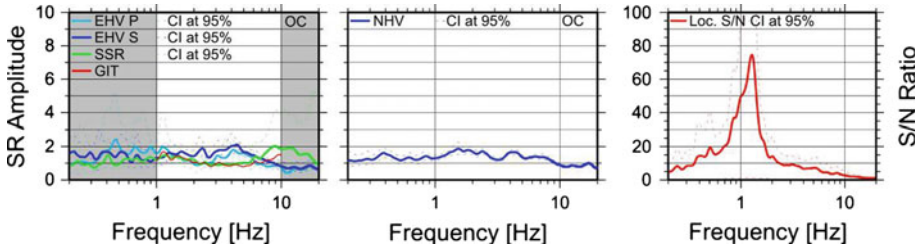

Fig. 20 Same as Fig. 13 but for site OC

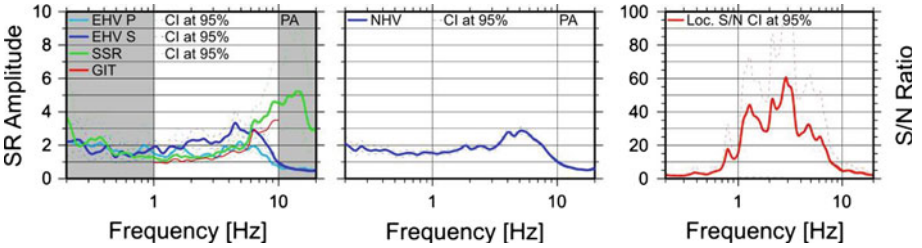

Fig. 21 Same as Fig. 13 but for site PA

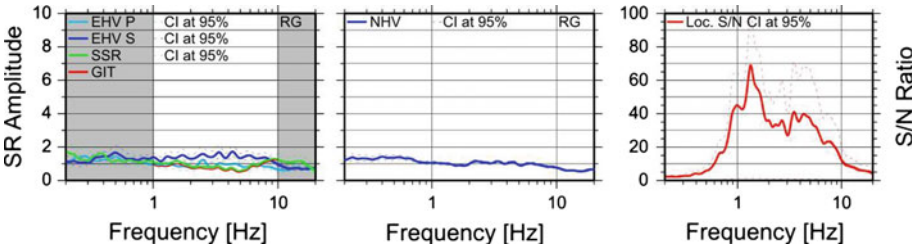

Fig. 22 Same as Fig. 13 but for site RG

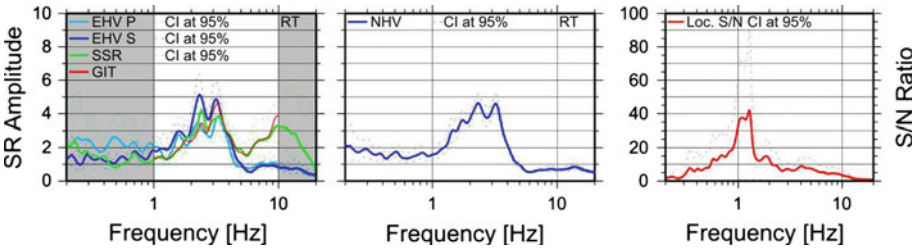

Fig. 23 Same as Fig. 13 but for site RT

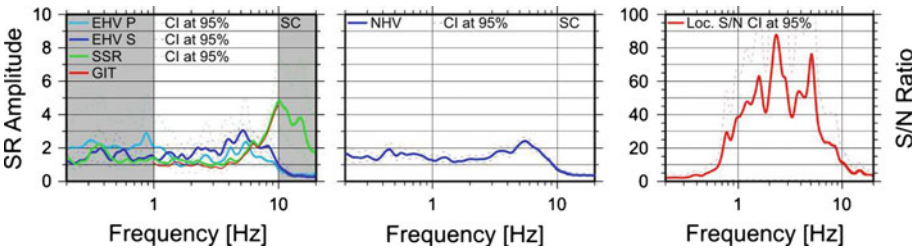

Fig. 24 Same as Fig. 13 but for site SC

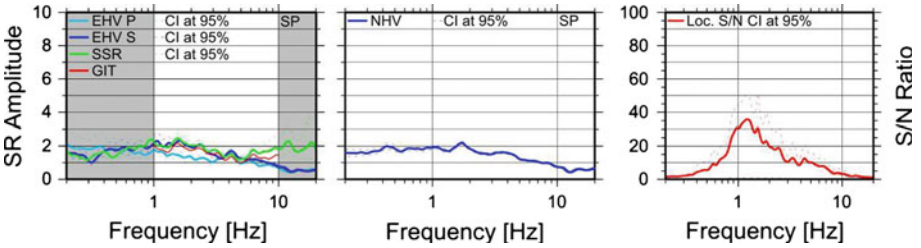

Fig. 25 Same as Fig. 13 but for site SP

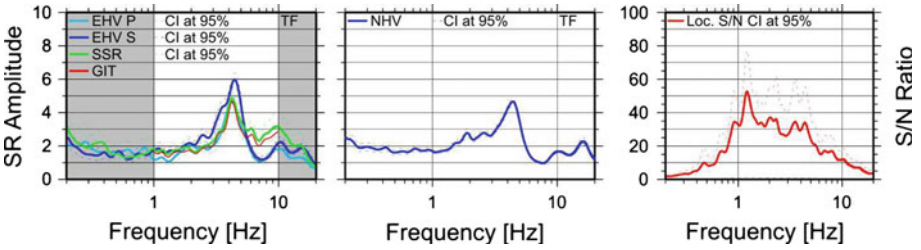

Fig. 26 Same as Fig. 13 but for site TF

References

Andrews DJ (1986) Objective determination of source parameters and similarity of earthquakes of different size. In: Das S, Boatwright J, Scholz CH (eds) Earthquake source mechanics. American Geophysical Union, Washington, pp 259–268

Bard PY (1995) Effects of surface geology on ground motion: recent results and remaining issues In: 10th European conference on earthquake engineering. Duma, Balkema, Rotterdam, pp 305–323

Bindi D, Parolai S, Cara F, Di Giulio G, Ferretti G, Luzi L, Monachesi G, Pacor F, Rovelli A (2009) Site amplifications observed in the Gubbio Basin, central Italy: hints for lateral propagation effects. Bull Seism Soc Am 99(2A): 741–760. doi:10.1785/0120080238

Bindi D, Parolai S, Grosser H, Milkereit C, Zunbul S (2006) Cumulative attenuation along source-to-receiver paths in northwestern Turkey. Bull Seism Soc Am 96(1):188–199. doi:10.1785/0120050037

Borcherdt RD (1970) Effects of local geology on ground motion near San Francisco Bay. Bull Seism Soc Am 60(1):29–61

Bragato PL, Laurenzano G, Barnaba C (2007) Automatic zonation of urban areas based on the similarity of H/V spectral ratios. Bull Seism Soc Am 97(5):1404–1412. doi:10.1785/0120060245

Caniani D, Pascale S, Sdao F, Sole A (2008) Neural networks and landslide susceptibility: a case study of the urban area of Potenza. Nat Hazards 45(1): 55–72. doi:10.1007/s11069-007-9169-3

Cara F, Di Giulio G, Milana G, Bordoni P, Haines J, Rovelli A (2010) On the stability and reproducibility of the horizontal-to-vertical spectral ratios on ambient noise: case study of Cavola, Northern Italy. Bull Seism Soc Am 100(3):1263–1275. doi:10.1785/0120090086

Castro RR, Anderson JG, Singh SK (1990) Site response, attenuation and source spectra of S waves along the Guerrero, Mexico, subduction zone. Bull Seism Soc Am 80(6A):1481

Castro RR, Gallipoli MR, Mucciarelli M (2004) An attenuation study in Southern Italy using local and regional earthquakes recorded by seismic network of Basilicata, online Available from. http://www.earth-prints.org/handle/2122/854. Accessed 16 September 2010

Chiauzzi L, Masi A, Mucciarelli M, Vona M, Pacor F, Cultrera G, Gallovic F, Emolo A (2011) Building damage scenarios based on exploitation of Housner Intensity derived from finite faults ground motion simulations. Submitted to Bull Earthquake Eng

Davis JC (1986) Statistics and data analysis in geology. 2. John Wiley and Sons (WIE), Toronto

Di Nocera S, Anagnostopoulos S, Pescatore T, Russo B, Senatore MR, Tramutoli M (1988) Note illustrative della carta geologica dell'alta valle del Basento (Appennino Lucano—Italia). In: Atti del Convegno: Ambiente fisico, uso e tutela del territorio di Potenza, Potenza

Dolce M, Masi A, Marino M, Vona M (2003) Earthquake damage scenarios of the building stock of Potenza (Southern Italy) including site effects. Bull Earthquake Eng 1(1):115–140
Field EH, Jacob KH (1995) A comparison and test of various site-response estimation techniques, including three that are not reference-site dependent. Bull Seism Soc Am 85(4):1127–1143
Gallipoli MR, Mucciarelli M, Šket-Motnikar B, Zupančić P, Gosar A, Prevolnik S, Herak M, Stipčević J, Herak D, Milutinović Z, Olumćeva T (2010) Empirical estimates of dynamic parameters on a large set of European buildings. Bull Earthquake Eng 8(3): 593–607. doi:10.1007/s10518-009-9133-6
Gavarini C, di Lavoro G (1999) Proposta di riclassificazione sismica del territorio nazionale. Ingegneria Sismica 1:5–14
Haghshenas E, Bard P, Theodulidis NSESAME WP04 Team (2008) Empirical evaluation of microtremor H/V spectral ratio. Bull Earthquake Eng 6(1):75–108. doi:10.1007/s10518-007-9058-x
Housner GW (1952) Spectrum intensities of strong motion earthquakes. In: The proceedings of the symposium of earthquake and blast effects on structures. Earthquake Engineering Research Institute, Los Angeles
INGV Macroseismic Database (n.d.) DBMI04, online Available from. http://emidius.mi.ingv.it/DBMI04/. Accessed 15 February 2011
INGV DPC-S3 (n.d.) DPC_INGV S3, online Available from. http://esse3.mi.ingv.it/. Accessed 16 September 2010
INGV Italian Hazard map (n.d.) Italian Hazard maps, online Available from. http://esse1.mi.ingv.it/. Accessed 16 September 2010
INGV-MEDnet (n.d.) MedNet—RCMT, online Available from. http://mednet.rm.ingv.it/rcmt.php. Accessed 21 September 2010
ISTAT demographic data (n.d.) ISTAT demographic data, online Available from. http://demo.istat.it/pop2009/index1.html. Accessed 17 September 2010
Itaca (n.d.) Itaca, online Available from. http://itaca.mi.ingv.it/ItacaNet/. Accessed 21 September 2010
Konno K, Ohmachi T (1998) Ground-motion characteristics estimated from spectral ratio between horizontal and vertical components of microtremor. Bull Seism Soc Am 88(1):228–241
Lahr JS (n.d.) HYPOELLIPSE Title and Contents Pages, online Available from. http://pubs.usgs.gov/of/1999/ofr-99-0023/. Accessed 14 September 2010
Lermo J, Chavez-Garcia FJ (1993) Site effect evaluation using spectral ratios with only one station. Bull Seism Soc Am 83(5):1574–1594
Lucente FP, Agostinetti NP, Moro M, Selvaggi G, Di Bona M (2005) Possible fault plane in a seismic gap area of the Southern Apennines (Italy) revealed by receiver function analysis. J Geophys Res 110(B4):B04307
Luzi L, Bindi D, Franceschina G, Pacor F, Castro RR (2005) Geotechnical site characterisation in the Umbria-Marche area and evaluation of earthquake site-response. Pure Appl Geophys 162(11):2133–2161. doi:10.1007/s00024-005-2707-6
Marcellini A, Pagani M (2004) Recent advances in earthquake geotechnical engineering and microzonation. Springer, Berlin
Masi A, Vona M, Mucciarelli M (2010) Selection of natural and synthetic accelerograms for seismic vulnerability studies on RC frames. J Struct Eng 1(1):136. doi:10.1061/(ASCE)ST.1943-541X.0000209
Molnar S, Cassidy JF (2006) A comparison of site response techniques using weak-motion earthquakes and microtremors. Earthquake Spectra 22(1):169–188. doi:10.1193/1.2160525
Moro M, Amicucci L, Cinti FR, Doumaz F, Montone P, Pierdominici S, Saroli M, Stramondo S, Di Fiore B (2007) Surface evidence of active tectonics along the Pergola-Melandro fault: A critical issue for the seismogenic potential of the Southern Apennines, Italy. J Geodynamics 44(12): 19–32. doi:10.1016/j.jog.2006.12.003
Nakamura Y (1989) A method for dynamic characteristics estimations of subsurface using microtremors on the ground surface. Q Rept Railway Tech Res Inst Jpn 30:25–33
Nogoshi M, Igarashi T (1971) On the amplitude characteristics of microtremor (part 2). J Seism Soc Jpn 24:26–40
NTC08 (n.d.) Consiglio Superiore Lavori Pubblici—Home, online Available from. http://www.cslp.it/cslp/. Accessed 30 September 2010
Oth A, Bindi D, Parolai S, Wenzel F (2008) S-Wave attenuation characteristics beneath the Vrancea region in Romania: new insights from the inversion of ground-motion spectra. Bull Seism Soc Am 98(5):2482–2497. doi:10.1785/0120080106
Parolai S, Bindi D, Augliera P (2000) Application of the generalized inversion technique (GIT) to a microzonation study: numerical simulations and comparison with different site-estimation techniques. Bull Seism Soc Am 90(2):286
Parolai S, Bindi D, Baumbach M, Grosser H, Milkereit C, Karakisa S, Zunbul S (2004) Comparison of different site response estimation techniques using aftershocks of the 1999 Izmit earthquake. Bull Seism Soc Am 94(3):1096

Parolai S, Richwalski SM (2004) The importance of converted waves in comparing H/V and RSM site response estimates. Bull Seism Soc Am 94(1):304

Pergalani F, Compagnoni M, Petrini V (2008) Evaluation of site effects using numerical analyses in Celano (Italy) finalized to seismic risk assessment. Soil Dyn Earthquake Eng 28(12):964–977. doi:10.1016/j.soildyn.2008.05.004

Pergalani F, Luzi L, Petrini V, Pugliese A, Romeo R, Sanò T (1999) Criteria for a seismic microzoning of a large area in central Italy. Soil Dyn Earthquake Eng 18:279–296

Rodriguez VH, Midorikawa S (2002) Applicability of the H/V spectral ratio of microtremors in assessing site effects on seismic motion. Earthquake Eng Struct Dyn 31(2):261–279

Steidl JH, Tumarkin AG, Archuleta RJ (1996) What is a reference site?. Bull Seism Soc Am 86(6):1733–1748

Strollo A, Parolai S, Jackel K, Marzorati S, Bindi D (2008) Suitability of short-period sensors for retrieving reliable H/V peaks for frequencies less than 1 Hz. Bull Seism Soc Am 98(2): 671–681. doi:10.1785/0120070055

Tryon RC (1939) Cluster analysis. McGraw-Hill, New York

Ueong YS (2009) A study on feasibility of SI for identification of earthquake damages in Taiwan. Soil Dyn Earthquake Eng 29(1):185–193

Wessel P, Smith WHF (1991) Free software helps map and display data. Eos Trans AGU 72:441–461